JP4J.2 A MODELING STUDY OF THE ALONG-FRONT PRECIPITATION VARIABILITY OF A PACIFIC NARROW COLD FRONTAL RAINBAND

Mei Han*
Goddard Earth Sciences and Technology Center, University of Maryland at Baltimore County, Baltimore, and Laboratory for Atmospheres, NASA Goddard Space Flight Center, Greenbelt, Maryland

Scott A. Braun
Laboratory for Atmospheres, NASA Goddard Space Flight Center, Greenbelt, Maryland

P. Ola G. Persson
Cooperative Institute for Research in Environmental Sciences, University of Colorado and NOAA/Environmental Technology Laboratory, Boulder, Colorado

Jian-Wen Bao
NOAA/Environmental Technology Laboratory, Boulder, Colorado

1. INTRODUCTION

The Tropical Rainfall Measuring Mission (TRMM) was designed to measure and monitor precipitation throughout the tropics using a combination of a precipitation radar (PR) and a microwave imager (TMI). TRMM data is currently being combined with data from other sensors to produce 3-h rain rates for both the tropics and midlatitudes. The Global Precipitation Measurement (GPM) mission, a constellation of existing and new satellites expected to be in place by 2010, will lead to an increased focus on midlatitude weather systems so that improving rain rate retrievals at higher latitudes will become increasingly important.

This paper investigates the distribution of precipitation associated with a midlatitude frontal system, which was observed by three consecutive overpasses of the TRMM satellite on February 19, 2001 during the Pacific Coastal Jets Experiment (PACJET). The TRMM observations revealed complex variations of the structures of a narrow cold frontal rainband (NCFR). The TMI brightness temperature suggests that, compared to the northern and southern ends of the rainband, more precipitation ice was present in the middle portion of the NCFR (where the front bowed out). Model simulations conducted using the Penn State University/National Center for Atmospheric Research mesoscale model (MM5) are examined to explain the distribution of precipitation associated with the NCFR.

2. OBSERVATIONS

The intense NCFR that is the subject of this study was associated with an occluded extratropical cyclone offshore of the U. S. western coast. In addition to TRMM observations, it was also sampled by the NOAA P-3 aircraft and the QuikScat satellite during the PACJET winter field campaign. Jorgensen et al (2003) analyzed the cores and gaps along the NCFR using aircraft observations and a model simulation. This paper focuses on a different aspect of the variation of the precipitation organization along this NCFR, namely the mesoscale to synoptic-scale variations along the front, which were observed by the TMI (~20 km horizontal resolution) and the PR (~4.5 km horizontal resolution).

Figure 1 shows the composite TMI brightness temperature at 19 GHz (TB19) and 85 GHz (TB85) and PR reflectivity from three different scans starting at 2342 UTC February 18 and ending at 0416 UTC February 19 2001. These pictures were put together by compositing with respect to a precipitation feature, seen in all three scans, in the TB19 observations (whose position is marked as the origin of the *x* and *y* axes) and simply overlaying the individual images. The high 19 GHz brightness temperatures are due to emission from precipitating liquid water, while the low 85 GHz brightness temperatures are due to scattering from precipitating ice (Hong et al 2000). An intense NCFR was revealed by the high value of TB19 in Fig. 1a. This band was up to 200 km wide and ~1000 km long. Its middle section bowed out and was associated with the highest values of brightness temperature at 19 GHz, which indicates the most intense precipitation. Figure 1b exhibits a region of low values of TB85 (shaded) in the middle, bowed portion of NCFR, suggesting a greater concentration of precipitating ice there. This area corresponds to a region between 33°N and 37°N from the TB85 plots of the individual scans (figures not shown). Figure 1c shows the reflectivity from PR observations. Since the swath width of the PR is less than a third of that of the TMI (Kummerow et al 1998), the reflectivity composite does not cover the whole area covered by the brightness temperature observations. The southernmost PR scan of the front lies ahead of its more northern counterparts because of a faster eastward propagation of the southern part of the front compared to that at the origin. The PR captured well the details of the precipitation structure in the bowed and southern portion of the NCFR. It shows a fairly typical structure of an intense NCFR, with the highest reflectivities located in the region where the TB85 values are lowest. Interestingly, this structure is also similar to a typical squall line with a leading convective

**Corresponding author address:* Mei Han, NASA GSFC, Code 613.1, Greenbelt, MD 20770; e-mail: han@agnes.gsfc.nasa.gov.

line preceding a precipitation minimum and a trailing stratiform precipitation region.

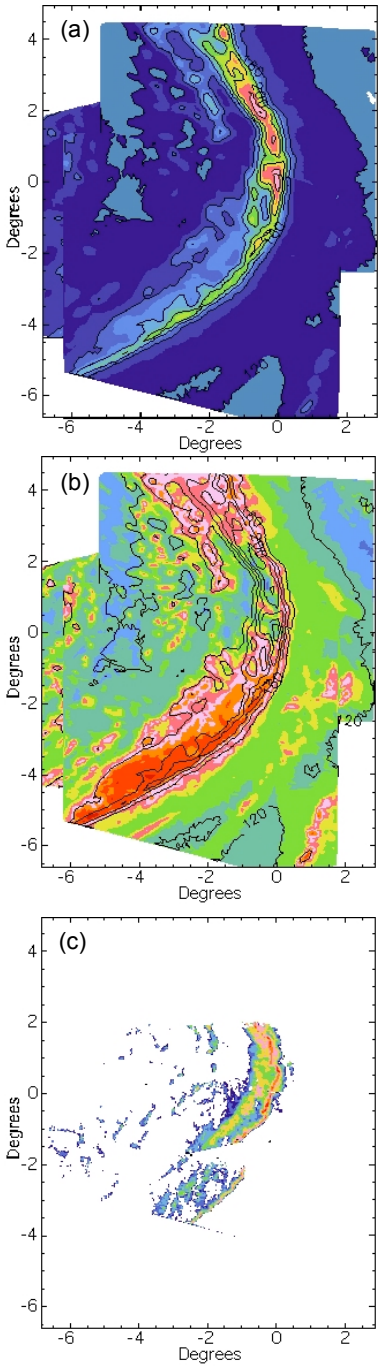

FIG. 1. Composite brightness temperature (K) from TMI at 19 GHz (contours and shades in a, contours in b) and 85 GHz (shades in b) and radar reflectivity (dBZ) from PR (c) from three scans starting at 2342 UTC February 18 and ending at 0416 UTC February 19 2001.

3. MODEL CONFIGURATION

The PSU-NCAR MM5 model (Version 3.6) is used to conduct a 48-h simulation of the NCFR from 0000 UTC 18 to 0000 UTC 20 February 2001. The model grid consists of four two-way nested domains. The outermost domain contains 100 × 85 grid points in *x* and *y* directions with a grid spacing of 45 km. The second domain contains 148 × 121 grid points with a grid spacing of 15 km. The third domain contains 199 × 199 grid points with a grid spacing of 5 km. The innermost domain contains 448 × 283 grid points with a grid spacing of 1.7 km. Fifty-one vertical sigma levels are used in each domain with 22 levels located below 850 mb. National Center for Environmental Prediction AVN-model analyses with 1° horizontal and 6-h temporal resolution are used to provide the initial and boundary conditions. The outer three domains are initialized at 0000 UTC 18 February 2001 and run for 48 hours, and the innermost domain is initialized at 1700 UTC 18 February and run for 22 hours.

Explicit cloud microphysics is treated with the Goddard microphysics scheme (Tao and Simpson 1993) for each domain. The Grell cumulus parameterization (Grell et al 1995) is applied in the 45-km and 15-km domains, while no cumulus scheme is used in the 5-km and 1.7-km domains. The Eta model PBL scheme is also used.

4. SIMULATION ANALYSIS

Figure 2 shows the model simulated radar reflectivity from the 5-km grid at 0200 UTC 19 February. The leading convective line is co-located with the leading edge of the narrow cold front identified from the equivalent potential temperature field (not shown). The location and shape of the NCFR agree well with the

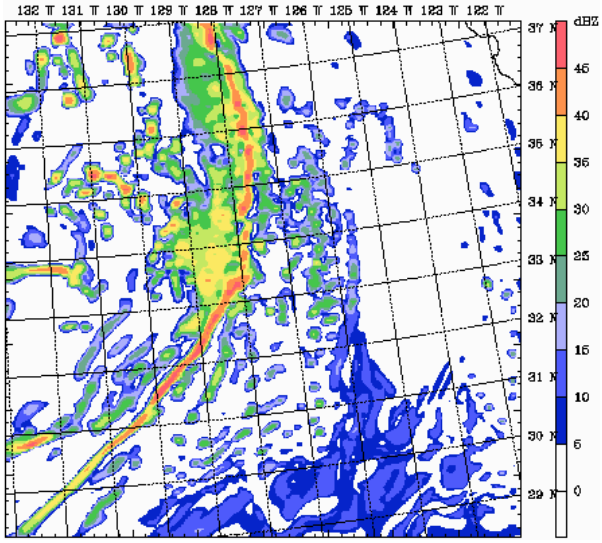

FIG. 2. Simulated radar reflectivity (dBZ) at the lowest model sigma level at 0200 UTC 19 February 2001.

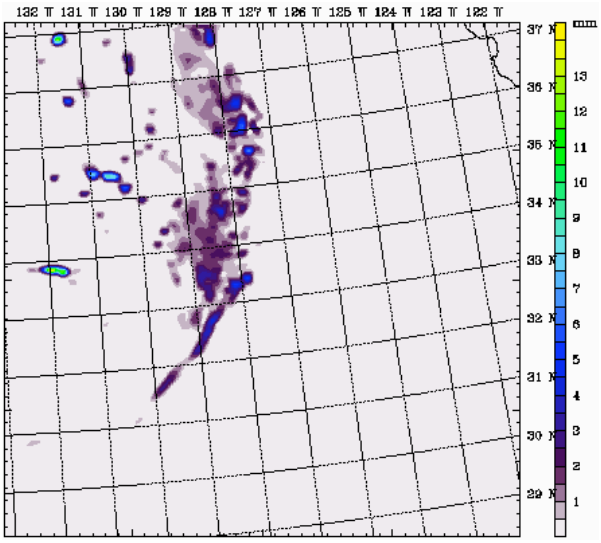

FIG. 3. Column-integrated graupel (mm) at 0200 UTC 19 February 2001.

observations (Fig. 1).

Along-front variations of the precipitation structure similar to those observed are clearly seen in the simulated reflectivity field. There is no trailing stratiform precipitation to the south of 33°N. Between 33°N and 37°N, where the band is somewhat bowed out, stratiform precipitation ~100-200 km wide follows the convective line. A broader view of the simulated reflectivity from the 15-km domain output (not shown) suggests that the stratiform precipitation diminishes toward the northern end of the NCFR, i.e. to the north of 37°N.

The structures of the simulated precipitation hydrometeors (rain, snow, and graupel) have been examined. Figure 3 shows the column-integrated graupel at 0200 UTC 19 February. The maximum concentration of the column-integrated graupel is ~5-6 mm and is generally located at the rainband's leading edge, which is consistent with the strong convective line shown in the reflectivity field. The trailing part of the column-integrated graupel is ~2-4 mm, corresponding to the stratiform precipitation region shown in Fig. 2. The overall region of large column-integrated graupel lies between 33°N and 37°N, which agrees well with the distribution of the precipitation ice implied in the TB85 field (Fig. 1b). Therefore, this high-resolution simulation successfully captured the along-front variations of precipitation associated with the NCFR. It is interesting, then, to explore the dynamical mechanisms responsible for the distribution of the precipitation, particularly the ice hydrometeors.

Figure 4 shows the smoothed simulated vertical motion (ω=*dp/dt*) from the 15-km domain at 0200 UTC 19 February. The maximum magnitude of the rising motion is ~ –21 and –30 dPa s^{-1} in the two centers near 128°W. The strong vertical motion is concentrated between 33°N and 38°N, which is consistent with the graupel concentrations in the middle portion of the NCFR.

Figure 5 shows potential vorticity (PV) and wind barbs at 300 mb at 0200 UTC 19 February. The white line indicates the position of the surface cold front. The high PV anomaly suggests the intrusion of stratospheric air and an upper-level front at its leading edge. An animation shows the upper-level front propagating eastward following the surface front. As the upper-level front moves eastward, positive PV advection occurs downstream near the bowed portion of the

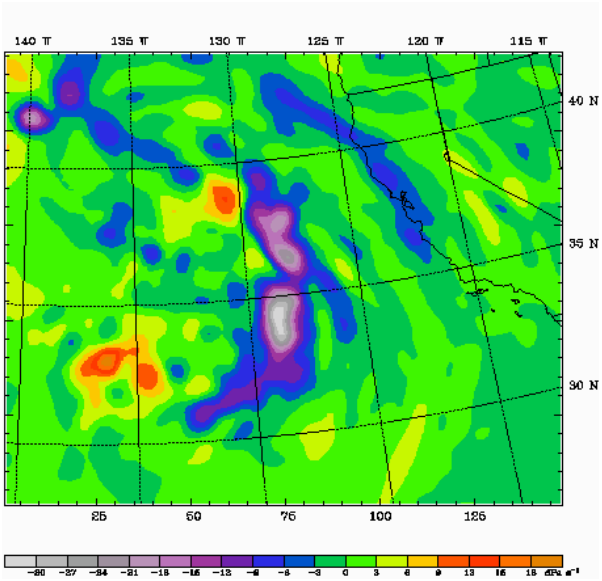

FIG. 4. Smoothed 500 mb vertical motion (dp/dt, dPa s^{-1}) at 0200 UTC February 2001

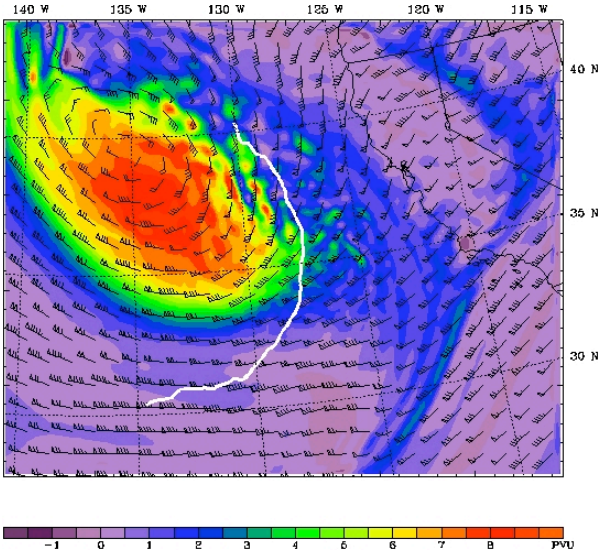

FIG. 5. Potential vorticity (PVU) and wind barbs at 300 mb at 0200 UTC 19 February 2001. Full barb is 5 m s^{-1}. The white thick line is portion of 306 K equivalent potential temperature field at 925 mb, indicating the position of the surface cold front.

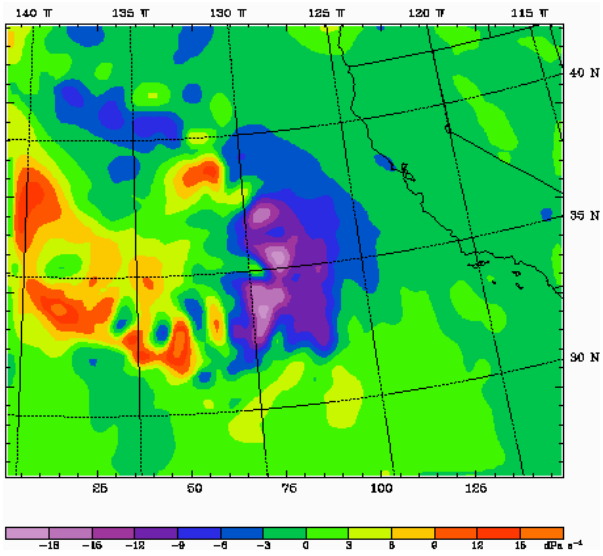

FIG. 6. Quasi-geostrophic omega (dPa s^{-1}) at 500 mb at 0200 UTC 19 February 2001.

surface front. This configuration suggests that the advancing upper-level front may play a role in the concentration of the precipitation ice in that area.

The quasi-geostrophic (QG) omega equation is solved to examine the vertical motion associated with the upper-level front. There is a broad area of upward motion (Fig. 6) due to QG forcing ahead of the upper-level front. The area with QG upward motion stronger than –6 dPa s^{-1} is concentrated between about 33°N and 37°N. This QG vertical motion distribution also agrees well with the smoothed vertical motion shown in Fig. 4. Therefore, the analysis strongly suggests that the presence of increased precipitation ice in the middle of the NCFR is due to PV advection associated with the advancing upper-level front.

5. CONCLUSIONS AND DISCUSSION

TRMM observations revealed significant along-front variations of the precipitation structure associated with a NCFR. Specifically, enhanced precipitation ice concentrations occurred along the middle portion of the rainband, where the cold front bowed out, compared to the southern and northern segments of the NCFR. A fine-scale MM5 simulation captured well the structure of the NCFR. The simulation confirmed that a large amount precipitation ice, i.e. graupel, occurred in the middle portion of the NCFR. Analysis of the simulation suggests that an advancing upper-level front played a key role in determining this structure. The potential vorticity advection associated with the upper-level front induced stronger QG upward motion along the middle portion of the NCFR than at its two ends. This intense upward motion led to deeper updrafts, enhanced condensation, and greater production of ice particles in that region.

Future research will compare the TRMM data and simulation output to aircraft observations of the front to study the finer-scale variations of the precipitation structure, including both the variations in the leading narrow convective line as well as variations in the trailing stratiform rain. Furthermore, relationships between observed and simulated microwave brightness temperatures and surface rainfall will be explored.

ACKNOWLEDGEMENTS

This work was supported by Dr. Ramesh Kakar at NASA Headquarters with funds from the NASA Precipitation Science program.

REFERENCES

Grell, G. A., J. Dudhia, and D. R. Stauffer, 1995: A description of the fifth-generation Penn State/NCAR Mesoscale Model (MM5). NCAR Tech. Note TN-398+STR, 122pp.

Hong, Y., J. L. Haferman, W. S. Olson, C. D. Kummerow, 2000: Microwave brightness temperatures from tilted convective systems. *J. Appl. Meteor.*, **39**, 983-998.

Jorgensen, D. P., Z. Pu, P. O. G. Persson, and W.-K. Tao, 2003: Variations associated with cores and gaps of a Pacific narrow cold frontal rainband. *Mon. Wea. Rev.*, **131**, 2705-2729.

Kummerow, C., W. Barnes, T. Kozu, J. Shiue, and J. Simpson, 1998: The tropical rainfall measuring mission (TRMM) sensor package. *J. Atmos. Oceanic Technol.*, **15**, 809-817.

Tao, W.-K. and J. Simpson, 1993: The Goddard Cumulus Ensemble Model. Part I: Model description. *Terr. Atmos. Oceanic Sci.*, **4**, 35-72.